Draft version November 11, 2014
Preprint typeset using LaTeX style emulateapj v. 04/17/13

arXiv:1408.5898v2 [astro-ph.HE] 10 Nov 2014

STRONGLY LENSED JETS, TIME DELAYS, AND THE VALUE OF H_0

Anna Barnacka[1,2], Margaret J. Geller[1], Ian P. Dell'Antonio[3], and Wystan Benbow[1]
[1]Harvard-Smithsonian Center for Astrophysics, 60 Garden St, MS-20, Cambridge, MA 02138, USA
[2]Astronomical Observatory, Jagiellonian University, Cracow, Poland
[3]Department of Physics, Brown University, Box 1843, Providence, RI 02912

Draft version November 11, 2014

ABSTRACT

In principle, the most straightforward method of estimating the Hubble constant relies on time delays between mirage images of strongly-lensed sources. It is a puzzle, then, that the values of H_0 obtained with this method span a range from $\sim 50-100\,\mathrm{km\,s^{-1}Mpc^{-1}}$. Quasars monitored to measure these time delays, are multi-component objects. The variability may arise from different components of the quasar or may even originate from a jet. Misidentifying a variable emitting region in a jet with emission from the core region may introduce an error in the Hubble constant derived from a time delay. Here, we investigate the complex structure of sources as the underlying physical explanation of the wide spread in values of the Hubble constant based on gravitational lensing. Our Monte Carlo simulations demonstrate that the derived value of the Hubble constant is very sensitive to the offset between the center of the emission and the center of the variable emitting region. Thus, we propose using the value of H_0 known from other techniques to spatially resolve the origin of the variable emission once the time delay is measured. We advocate this method particularly for gamma-ray astronomy, where the angular resolution of detectors reaches approximately 0.1 degree; lensed blazars offer the only route for identify the origin of gamma-ray flares. Large future samples of gravitationally lensed sources identified with Euclid, SKA, and LSST will enable a statistical determination of H_0.

Subject headings: Galaxies: active – gravitational lensing: strong –gamma-rays: jets

1. INTRODUCTION

The Hubble constant, H_0, is a fundamental cosmological parameter. A rich variety of observational methods yield remarkably precise values of this parameter (Freedman & Madore 2010). For example, the Cepheid distance ladder gives $73.8\pm2.4\ \mathrm{km\,s^{-1}Mpc^{-1}}$ (Riess et al. 2011a,b).

In principle, gravitational lensing provides an independent one-step method for Hubble constant determination. This approach was first proposed by Refsdal (1964), who suggested using time delays between the images of gravitationally-lensed supernovae long before discovery of the first gravitationally lensed quasar (Walsh et al. 1979). The time delays are proportional to H_0^{-1} and weakly depend on other cosmological parameters (Refsdal 1964; Schechter et al. 1997; Treu & Koopmans 2002; Kochanek 2002; Koopmans et al. 2003; Oguri 2007; Suyu et al. 2013b; Sereno & Paraficz 2014).

Initially, the practical implementation of the time delay method suffered from a number of challenges (Courbin 2003; Kochanek & Schechter 2004; Schechter 2005). The accuracy of the method relies on the precision of the time delay determination, knowledge of the redshifts in the system and reconstruction of the mass distribution of the lens. Long-term monitoring of gravitationally-lensed quasars provides time delays with uncertainties of a few percent (Fassnacht et al. 2002; Eulaers & Magain 2011; Rathna Kumar et al. 2013; Tewes et al. 2013b; Eulaers et al. 2013). Advances in spectroscopy combined with precise cosmology allow for distance measurement with great accuracy. The mass distribution of the lens can be reconstructed well using resolved radio and optical images. In addition, for lenses located at a low enough redshift, the velocity dispersion of the lens can be measured, which allows for independent confirmation of the mass distribution (Bolton et al. 2008).

To date, dozens of gravitationally-lensed systems yield measured time delays. Lens modeling of these systems provides estimates of the Hubble constant covering a large range from $\sim$ 50 to $\sim$ 100 $\mathrm{km\,s^{-1}Mpc^{-1}}$ (Rathna Kumar et al. 2014; Paraficz & Hjorth 2010; Fassnacht et al. 1999). It is puzzling that these estimates of the Hubble parameter derived from time delays span a range much larger than expected from other precise astrophysical methods.

Measurements of time delays are based on monitoring variable sources. The variability of quasars has been known for a long time (Matthews & Sandage 1963). The variability of quasars can be described well by a damped random walk (MacLeod et al. 2010; Kozłowski et al. 2010) and the optical flux fluctuations are interpreted as thermal fluctuations driven by an underlying stochastic process (Kelly et al. 2009).

The amplitude of variability in radio-quiet quasars is usually small. Sesar et al. (2007) reported that at least 90% of quasars are variable at the 0.03 mag level (rms) on timescales up to several years, and that 30% of quasars are variable at the 0.1 mag level. The variability of gravitationally-lensed quasars selected for monitoring by COSMOGRAL[1] is typically in the range from 0.2 to even 2 mag.

Monitoring of lensed systems focuses on radio-loud

abarnacka@cfa.harvard.edu

[1] the COSmological MOnitoring of GRAvItational Lenses: http://cosmograil.epfl.ch/

quasars, which constitute about 20% of the quasar sample. The emission of radio-loud quasars is not limited to thermal emission from the accretion disk; the majority of the variable emission may originate from relativistic jets.

These jets are the largest particle accelerators in the universe, producing radiation from radio up to very high energy gamma-rays. Observations of jets from radio to x-ray wavelengths, where the sources are resolved, reveal that the jets have very complex structure composed of bright knots, blobs and filaments, with sizes ranging from the subparsecs up to dozens of kpcs (Harris & Krawczynski 2006; Tavecchio et al. 2007; Siemiginowska et al. 2002; Marscher et al. 2008; Biretta et al. 1991). The source variability can be very complex. Variable emission may originate from different components close to the core, or it can originate from the knots along the jet as in the well studied example of M87 (Harris et al. 2006).

If the projected distance between the central part of a quasar and the variable emission sites along a jet are even 1% of the Einstein radius, which corresponds typically to $\sim 30\,\mathrm{pc}$, time delays and magnification ratios between the images may differ significantly. These differences, in principle, can be used to investigate the structures of jets at high energies, where the emission cannot be spatially resolved due to the poor angular resolutions of the detectors (Barnacka et al. 2014a,b). Conversely, the multiple emitting regions of quasars can affect the determination of the Hubble constant.

Here, we investigate the impact of the complex structure of the source on Hubble parameter determination. We summarize the current Hubble parameter measurement in § 2. To demonstrate how estimates of the Hubble constant vary with the projected distance between the core and the emitting region within the jet, we build a toy model of the M87 jet, which we describe in § 3. We give an overview of strong gravitational lensing phenomena in § 4, and perform Monte Carlo simulation in § 5. We discuss the results of simulations in § 6. We summarize existing lensing measurements of H_0 (§ 6.1). Then, in § 6.2, we propose to use a Hubble parameter tuning method to elucidate the spatial origin of variable emission. We discuss the application of the Hubble parameter tuning approach to high-energy astronomy in § 6.3. We conclude in § 7.

2. HUBBLE CONSTANT

The current era of high-precision cosmology provides measurements of the Hubble constant, H_0, with a remarkably small error. For example, the modeling of Planck observations of the cosmic microwave background fluctuations using the flat-ΛCDM cosmological model gives $H_0 = 67.3 \pm 1.2\ \mathrm{km\,s^{-1}\,Mpc^{-1}}$ (Planck Collaboration et al. 2013).

Many independent methods provide a measure of H_0. Examples include the Hubble Space Telescope Key Project which provided a $H_0 = 72 \pm 8\ \mathrm{km\,s^{-1}Mpc^{-1}}$ (Freedman et al. 2001). The Cepheid distance ladder gives $73.8 \pm 2.4\ \mathrm{km\,s^{-1}Mpc^{-1}}$ (Riess et al. 2011a,b) and $74.3 \pm 1.5\,(\mathrm{statistical}) \pm 2.1\,(\mathrm{systematic})\,\mathrm{km\,s^{-1}\ Mpc^{-1}}$ (Freedman et al. 2012).

One of the most straightforward methods of estimating the value of H_0 relies on time delays between images of strongly-lensed sources. This method has the advantage of being independent of the local distance ladder. However, individual lens systems yield varied results (see Table 1). Fadely et al. (2010) plot the H_0 obtained for the well-observed set of individual lens systems. Roughly half of the studies are consistent with $H_0 < 60\ \mathrm{km\,s^{-1}Mpc^{-1}}$, well outside the limits from other measures. The rest scatter across the range $H_0 = 65 - 80\ \mathrm{km\,s^{-1}Mpc^{-1}}$. Thus these measurements present a puzzle and a challenge to understand the astrophysics that might underlie the varying results.

Studies of Q0957+561 (Bernstein & Fischer 1999; Keeton et al. 2000) result in $H_0 > 85\ \mathrm{km\,s^{-1}Mpc^{-1}}$, and studies of PKS 1830-211 result in values across the range $H_0 = 44 - 76\ \mathrm{km\,s^{-1}Mpc^{-1}}$(Lidman et al. 1999; Lehár et al. 2000; Winn et al. 2002; Barnacka 2013). Both of these systems host powerful jets. More recently, Fadely et al. (2010) analyzed HST data for Q0957+561 and identified 24 new strongly lensed features, which they use to constrain a mass model for the lens. Adopting the radio time delay measured with an error $\lesssim 1\%$, they found $H_0 = 79.3^{+6.7}_{-8.5}\mathrm{km\,s^{-1}Mpc^{-1}}$. Fadely et al. (2010) then concluded that the quasar flux ratio predicted by

TABLE 1
HUBBLE CONSTANT MEASUREMENTS FOR INDIVIDUAL GRAVITATIONALLY LENSED SOURCES.

Object	Hubble constant	References
HE 0435-1223	91.9 ± 17.1	Rathna Kumar et al. (2014)
	62 ± 5	Courbin et al. (2011a)
RX J0911.4+0551	79.3 ± 32.6	Rathna Kumar et al. (2014)
	71 ± 12	Hjorth et al. (2002)
SBS 0909+532	81.9 ± 20	Tian et al. (2013)
FBQ 0951+2635	60 ± 9	Jakobsson et al. (2005)
Q0957+561	50 ± 17	Rhee (1991)
	77 ± 29	Bernstein & Fischer (1999)
	79.3 ± 7	Fadely et al. (2010)
	97.3 ± 31.4	Rathna Kumar et al. (2014)
SDSS J1004+4112	91.8 ± 30.4	Rathna Kumar et al. (2014)
HE 1104-1805	62 ± 4	Gil-Merino et al. (2002)
PG 1115+080	59 ± 12	Treu & Koopmans (2002)
	57 ± 7	Tortora et al. (2004)
	61.5 ± 19.5	Rathna Kumar et al. (2014)
RX J1131-1231	71.6 ± 25.4	Rathna Kumar et al. (2014)
	$78.7^{+4.3}_{-4.5}$	Suyu et al. (2013b)
SBS 1520+530	58.3 ± 17.3	Rathna Kumar et al. (2014)
B1600+434	74 ± 14	Koopmans et al. (2000)
B1608+656	63 ± 15	Fassnacht et al. (2002)
	75 ± 6	Koopmans et al. (2003)
	69.7 ± 5	Suyu et al. (2010)
	60.3 ± 11.2	Rathna Kumar et al. (2014)
SDSS J1650+4251	51 ± 7	Vuissoz et al. (2007a)
WFI J2033-4723	63 ± 5	Vuissoz et al. (2008a)
	71.5 ± 12.2	Rathna Kumar et al. (2014)
B 0218+357	69 ± 15	Biggs et al. (1999)
	76 ± 7	Lehár et al. (2000)
	78 ± 6	Wucknitz et al. (2004)
	61 ± 7	York et al. (2005)
	64 ± 4	Cheung et al. (2014)
PKS 1830+211	76 ± 18	Lidman et al. (1999)
	73 ± 35	Lehár et al. (2000)
	44 ± 9	Winn et al. (2002)
	48.7 ± 13.7	Barnacka (2013)
HE 2149-2745	86.8 ± 33.5	Rathna Kumar et al. (2014)
	65 ± 8	Burud et al. (2002)

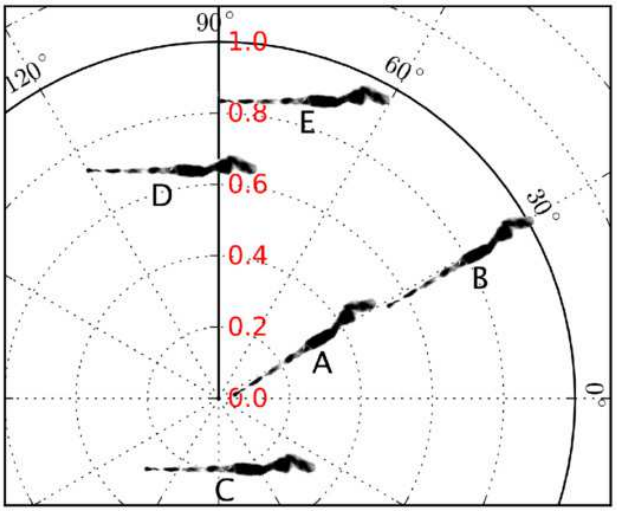

FIG. 1.— Example alignments of jets in the source plane. The radial coordinates indicate the distance from the center of the lens mass normalized by the Einstein radius.

their detailed lens model is inconsistent with existing radio measurements again indicating that there is some poorly understood underlying astrophysics.

Another system, B0218+357, "a golden lens" for H_0 measurement (Wucknitz et al. 2004), also hosts a powerful jet. The H_0 values based on this systems are in the range 61-78 $\mathrm{km\,s^{-1}Mpc^{-1}}$ (York et al. 2005; Cheung et al. 2014; Lehár et al. 2000; Wucknitz et al. 2004). The most recent attempt to measure H_0 for this system, using the time delay of 11.46 ± 0.16 days from gamma-ray emission, results in a Hubble constant of 64 ± 4 $\mathrm{km\,s^{-1}Mpc^{-1}}$ (Cheung et al. 2014).

Schneider & Sluse (2013, 2014) investigated the impact of mass-sheet degeneracies on the predictions of the Hubble constant and found that these mass-modeling errors could lead to deviations of up to 20% on the Hubble constant. Suyu et al. (2013a) investigate the tension between the H_0 obtained using gravitational lensing and the Planck results. They revise analysis of the gravitational lens RXJ1131-1231, reducing the systematic errors introduced by an assumed lens model density profile. They emphasize that the tension in H_0 measurements from different methods could be due to unknown systematic uncertainties.

The observational situation presents a mystery. The straightforward application of lensing time delays produces an array of results for the Hubble constant that are often substantially offset from those obtained with other standard methods. The scatter among the lensing results is also remarkably large. Previous attempts to explore the scatter in the values of H_0 from individual lenses have assumed sources that vary uniformly, so that the centroid of the light distribution is also the centroid of the variability. We investigate the structure of the sources as an explanation for these puzzling results.

3. TOY MODEL: LENSED JET

Here we introduce a toy model of a strongly lensed source to investigate the impact of complex source structure on H_0 estimation. As an inspiration for the source model, we use the nearest and best studied active galactic nucleus with a relativistic jet, M87.

M87 is a local example of a source with very complex variability (Aharonian et al. 2006; Abramowski et al. 2012). Spatially-resolved observations of M87 reveal that variable emission may originate from at least two locations: the core and the HST-1 knot embedded within the jet. The core refers to the central region of the active galactic nucleus. Commonly the term "core" is defined as the position of the brightest feature in VLBA images of blazars (Lobanov 1998; Marscher 2008; Pushkarev et al. 2010). The core and HST-1 have a projected separation of ∼60 pc (Biretta et al. 1999). The M87 jet also has many bright knots at much greater distances than HST-1.

During the flaring activity of M87 observed by the Chandra satellite in 2004/2005, the x-ray flux from HST-1 increased by a factor of 50 (Harris et al. 2006); thus demonstrating that the variability can originate from different parts of the jet. The locations of the variable emission can be hundreds of parsecs away from the central engine.

M87 is located at 16 Mpc (Tonry 1991); thus the separation between the emitting regions of 60 pc corresponds to 0.7 arcseconds. The angular resolution of the Chandra satellite is 0.5 arcseconds[2], allowing discrimination between emission from HST-1 and from the core. If we imagine an M87 analog located at 1 Gpc from the observer, this separation would correspond to 0.01 arcseconds. The emission would be unresolved in the x-rays and it would be challenging to resolve even with HST.

Lensed sources are usually located at distances greater than 1 Gpc. The M87 example demonstrates that variability originating from regions along the jet could easily be misinterpreted as emission from the core.

The angular separation between the core and knots along the jet depends on the viewing angle to the jet and the distance of the knot from the core. The emission from the jet is relativistically boosted when the jet is pointed at a small angle ($\lesssim 20°$ - $30°$) relative to the line of sight between the source and the observer. The viewing angle for a typical radio-loud quasars is $< 5°$, for BL Lacs objects it is $< 10°$, and it is $< 50°$ for the radio galaxies (Lähteenmäki & Valtaoja 1999). The viewing angles for a sample of the brightest *Fermi*/LAT detected blazars derived from high-resolution VLBA images range from 1° to 5° (Savolainen et al. 2010). The M87 jet is observed at $\sim 15°$ relative to the line of sight (Biretta et al. 1999; Perlman et al. 2011); it is thus representative of the range of observed sources.

Luminous knots may be located even hundreds of kpcs from the central engine (Massaro et al. 2011). Thus, even when the viewing angle is small, of the order of a few degrees, the angular separation between distant knots along the jet may constitute a significant fraction of the Einstein radius of the lens, or may extend beyond it.

The geometry of the sources can be very complex. There are also many different configurations of the source-lens-observer systems. However, in the source plane, the parameter space that adequately describes these sources reduces to the separation between the core and the variable knot. In our toy model we randomly

[2] http://cxc.cfa.harvard.edu/cdo/about_chandra/overview_cxo.html

select both the position of the core in the source plane, and the alignment of jet relative to the core. We investigate the resulting changes in the time delay and the magnification ratios.

To investigate the impact of source structure on the determination of H_0 further, we consider an M87-like source, located at redshift $z_S = 2.5$, and a lens at redshift $z_L = 0.89$. Our choice of lensing system is motivated by the observed case of the gravitationally-lensed blazar PKS 1830-211, where gamma-ray emission was used for the first time to investigate gravitational lensing at high energies (Barnacka et al. 2011). We consider what happens to the value of H_0 as we vary the projected distance between the core and the variable emitting region along the jet. We set the mass of the lens so that the Einstein radius for a source at z=2.5 is 0.4".

The measured quantities include the distance ratio, the time delay, the magnification ratio, and the morphology of the lensed images. The distance ratio is a ratio of angular distances,

$$D \equiv \frac{D_{OL} D_{OS}}{D_{LS}}\,, \tag{1}$$

where the distance from the observer to the lens is D_{OL}, the distance from the observer to the source is D_{OS}, and the distance from the lens to the source is D_{LS}. We calculate distances based on a homogenous Friedmann-Lemaître-Robertson-Walker cosmology, with $H_0 = h\times$ 100 km/s/Mpc, where $h = 0.673$, the mean mass density $\Omega_M = 0.315$ and the normalized cosmological constant $\Omega_\Lambda = 0.686$ (Planck Collaboration et al. 2013).

The magnification ratio and the time delay both change with the distance between the emitting regions in the source plane. Differences in the projected orientation of the jet in the source plane also impact the magnification ratio and time delay.

As specific examples of the effects that source structure and orientation can have on H_0, we first consider five different jet locations and alignments in the source plane (Figure 1). We model the lens as a singular isothermal sphere and we compute differences in magnification ratios and time delays as a function of projected distance between the emitting regions. We then demonstrate the impact of these variations on the estimation of H_0.

4. STRONG GRAVITATIONAL LENSING

Here we investigate the five examples of Figure 1 in detail. We review the elements of the lensing model and we demonstrate the substantial effects of source structure on the value of H_0 derived from the measured time delay.

Light rays from a source in the presence of matter are deflected by an angle α before reaching an observer. In the thin-lens approximation, the rays are deflected by an angle of

$$\vec{\alpha} = \bigtriangledown\psi(\vec{\theta})\,, \tag{2}$$

where $\psi(\vec{\theta})$ is the effective gravitational potential of the lens at an image position $\vec{\theta}$.

Using simple geometry (see Narayan & Bartelmann 1996; Barnacka 2013), the lens equation is

$$\vec{\beta} = \vec{\theta} - \vec{\alpha}(\vec{\theta})\,, \tag{3}$$

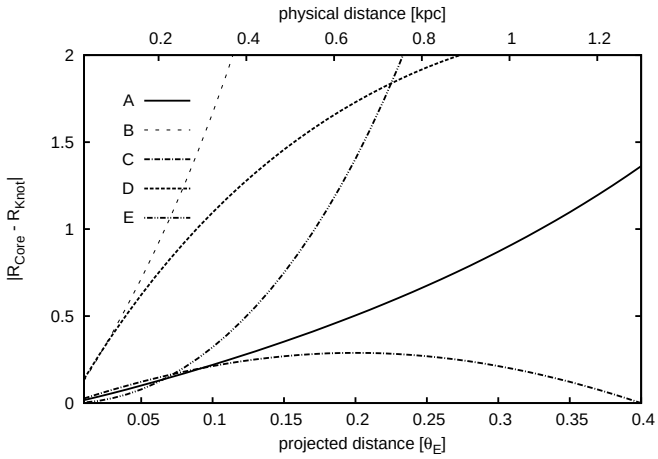

FIG. 2.— Difference in magnification ratio between the core and the knot as a function of projected distance between them. The figure shows the absolute value of the difference in the magnification ratio. The projected distance between the core and the knots is presented in Einstein radius units (bottom), and in physical units corresponding to the source plane (top).

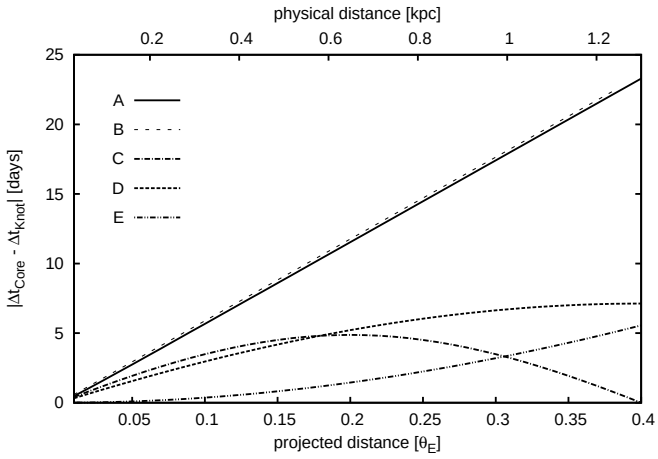

FIG. 3.— Difference in time delay between the core and the knot along the jet as a function of projected distance between them.

where $\vec{\beta}$ is the position of a source in the image plane. The lens equation is generally not linear. Thus, multiple images, $\vec{\theta_\pm}$, corresponding to a single source position can be produced.

The time delay function can be obtained from Fermat's principle:

$$\frac{c\,\Delta t(\vec{\theta})}{(z_L+1)} = D\left[\frac{1}{2}(\vec{\theta}-\vec{\beta})^2 - \psi(\vec{\theta})\right]\,, \tag{4}$$

where Δt is the time delay, and c is the speed of light. The distance ratio D is inversely proportional to H_0, thus equation (4) provides a direct route to the Hubble constant parameter once the time delays are measured.

The time delay is proportional to the square of the angular offset between $\vec{\theta}$ and $\vec{\beta}$. Therefore, different time delays result when emission originates from different regions, for example, a core or knots along a jet.

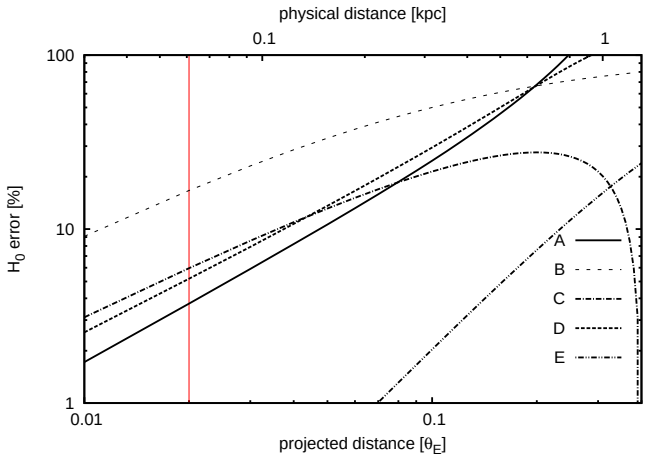

FIG. 4.— Deviation of the derived Hubble parameter as a function of the projected distance between the core and the emitting region within the jet. The error is calculated as (H-H_0)/H_0, where H_0 is a real value of the Hubble constant. H is the value of the Hubble constant calculated using the position of the core, and the time delay originating from the emitting region along the jet at a given projected distance from the core. The perpendicular line indicates the projected distance between the core and HST-1 observed in M87.

Light deflection in a gravitational field not only delays the rays, but also magnifies the sources. These magnifications are given by the determinant of the Jacobian matrix of the lens mapping $\theta \rightarrow \beta$. The magnification factor is

$$A = \left| \det \frac{\partial \beta}{\partial \theta} \right|^{-1} . \tag{5}$$

The magnification A is the ratio between the flux of an image and the flux of the unlensed source. If a source is mapped onto several images, the ratios of the respective magnification factors are equal to the flux ratios of the images (Schneider et al. 1992).

We use the singular isothermal sphere (SIS) profile to characterize the lens. This model is the simplest parameterization of the spatial distribution of matter in astronomical systems like galaxies and clusters of galaxies. In general, the mass distribution of the lens composed of stellar and dark matter is well represented by an isothermal model over many orders of magnitude in radius, and deviate significantly only far outside the Einstein radius where it is not relevant for our results. The SIS model is consistent with the results of the Sloan Lens ACS Survey (Gavazzi et al. 2007; Auger et al. 2010).

The lensing potential of the SIS is defined as

$$\psi(\theta) = \frac{D_{LS}}{D_{OS}} \frac{4\pi\sigma^2}{c^2} |\theta| , \tag{6}$$

where σ is a velocity dispersion.

Using this lensing potential, equations (2) and (3), the image position is

$$\theta_\pm = \beta \pm \theta_E , \tag{7}$$

where θ_E is the Einstein radius.

The magnification ratio between images, $A_\pm$, is

$$R = \frac{A_+}{A_-} = \frac{\theta_+}{\theta_-} , \tag{8}$$

and the time delay for $\beta > 0$ is

$$\frac{c\Delta t}{(1+z_L)} = D\theta_E(\theta_E - (|\theta_+| - |\theta_-|)) . \tag{9}$$

Figure 2 shows the difference in the magnification ratio between the core and the emitting region along the jet as a function of the projected distance between them. Figure 3 shows the difference in the time delays for the same configurations. The complex structure of the source produces significant differences in both the time delays and magnification ratios. For example, emitting regions separated by a projected distance of 5% of the Einstein radius produce a difference in the magnification ratios in the range 0.1 to 0.7 depending on the alignment in the source plane. In our model 5% of the Einstein radius corresponds to a projected distance of $\sim$ 160 pc. For the same projected distance the change in the time delay ranges from 1 to 3 days.

The rate of change of the lens parameters depends on the jet alignment in the source plane (see Figures 2 and 3). The largest rate of change in time delay and magnification ratios occurs when the jet is oriented along the radial direction in the source plane.

Figure 4 shows the absolute value of the normalized difference between the true Hubble parameter H_0, and the value of the Hubble parameter, H, calculated using the position of the core and the time delay originating from the emitting region along the jet. The departures from the true value arise from misinterpreting the location of the variable emitting region. In other words, they arise from the assumption that the variable emitting region is always the same and that it is the core. Even for a small separation between the true variable emission region and the core of $\sim$60 parsecs, the deviation between the derived Hubble parameter and the true value can be as large as 20%.

For powerful jets, the projected separation between the core and an emitting regions along the jet can be as large as hundreds of kpcs. Note that for some jet alignments (e.g. A and D), the deviation of the H_0 measurement from the true value can become as large as 100% for separations of 20% of the Einstein radius. In the toy model $\sim$600 parsecs is $\sim$20% of the Einstein radius.

5. MONTE CARLO SIMULATIONS

The five examples we have explored thus far demonstrate the remarkable impact of source structure on the Hubble parameter derived from time delays of strongly-lensed sources. The next goal is to compare the basic model with existing observations.

In this section, we explore the existing measurements of H_0 determined from strongly-lensed sources. We take the measurements at face value and we compare the distribution of these measured values with a Monte Carlo simulation that samples the full source plane for a set of sources with a variety of projected distances between the varying emission region and the core.

Figure 5 shows a compilation of the measurements (Table 1). Note the broad distribution of the individual measurements scattering in the range from 40 to 100. The distribution of H_0 shows an underrepresented number of measurements around 67. This value corresponds to the H_0 reported by Planck (Planck Collaboration et al.

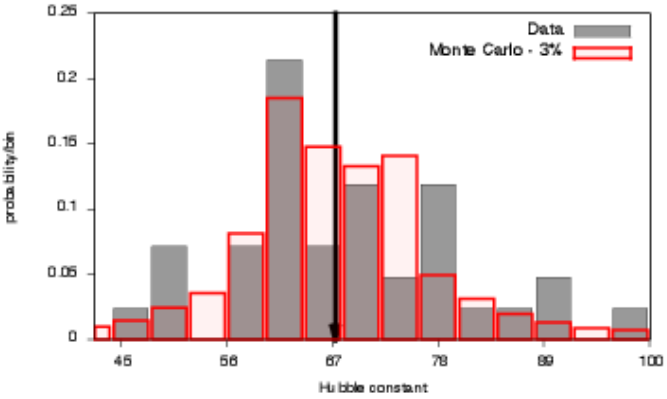

FIG. 5.— Gray distribution represents Hubble constant measurements summarized in table 1. Red distribution is the results of Monte Carlo simulations of 4000 trials, assuming distance between the core and variable emitting region of 3% of Einstein radius. Black line indicates the Planck satellite estimation of 67.3.

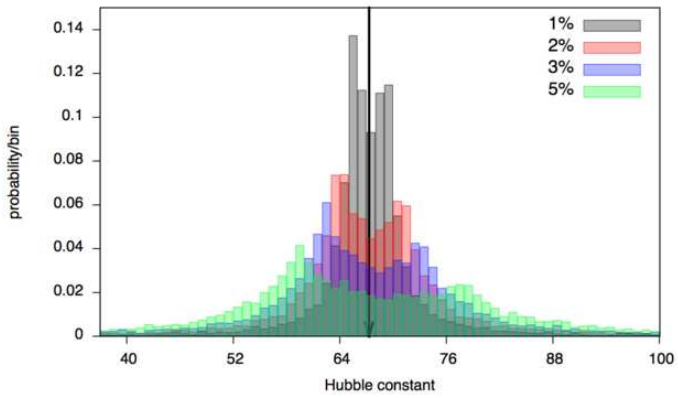

FIG. 6.— Distributions of the Hubble constant obtained with the Monte Carlo simulation assuming different distances between the quasar and the emitting region along the jet. Black line indicates the Planck satellite estimation of 67.3.

2013). The distribution has preferred values below 64, and broad scatter for values above 70.

5.1. *Model*

We ask whether a model based on simple assumptions about the structure of the sources can reproduce the salient features of the observed distribution of lensing H_0 values. In the simplest model, the location of a quasar and the alignment of its jet are both random in the source plane. We perform Monte Carlo simulations by randomly selecting the position of a quasar in the source plane. For each quasar position, we also randomly select the jet alignment. Then, we compute H_0 for a source located at the position of the quasar and we compute the time delay that corresponds to a variable emission region positioned along the jet, rather than in the core. Figure 6 shows the distributions of H_0 for distances between the quasar and variable emitting region along the jet that correspond to 1%, 2%, 3% and 5% of the Einstein radius. We simulate 10^5 sources for each separation.

We assume an H_0 of 67.3 to calculate time delays. The recovered average value of H_0 from the distributions is $\sim 67.2-67.4$. The effect of the misinterpreted position of the source cancels out in the mean when large numbers of measurements from gravitationally-lensed systems are averaged. For any individual source, the deviation from the true value can be large.

5.2. *Bimodal Distribution*

The simulated distribution of H_0 has a distinctive bimodal character. This bimodality is a consequence of the geometry, and the change of lens parameters across the source plane. The position of the images and the time delay change with the distance from the center of the lens mass distribution (see equations (7) and (9)). The alignment of the jet in the source plane is random. The distance of the variable emitting region from the center of the lens mass distribution can be either smaller or larger than the distance between the quasar and the center of the lens mass distribution. Thus, the values of H_0 are either over or underestimated (Figures 7 and 8).

The chance that the jet will be aligned in such a way that the emitting region along the jet and the core are at the same distance from the center of the lens is small. Therefore, the simulated distribution of H_0 shows that the nominal value is underrepresented in the distribution. On other words, there is a dip in the center of the distribution of recovered values of H_0.

The Root-Mean-Square (RMS) of the H_0 distribution increases with projected separation between the variable emission source and the core. For distances between the core and an emission region along the jet corresponding to 1%,2%, 3% and 5% of the Einstein radius, the corresponding spread in the Hubble parameter is 5.65, 7.92, 9.56, and 12.29 [$\mathrm{km\,s^{-1}Mpc^{-1}}$], respectively. The scatter in H_0 reflects the offset between the position of the variable emitting region and the assumed position of the core. Thus, the RMS of measured H_0 together with true value of H_0 determine the most likely offset between the core and the variable emitting region.

5.3. *Position of the Source*

The value of H_0 is clearly very sensitive to the position of the source. Figures 7 and 8 show examples where the core is located at 0.35 Einstein radius and 0.7 Einstein radius from the center of the lens mass, respectively. The scale shows how the estimated Hubble parameter changes when the variable emission originates at a particular distance from the core. Figures 7 and 8 explore distances between the core and emitting region along the jet only up to $\sim 5\,\%$ of the Einstein radius. Even for very small distances, like 2.5% of Einstein radius, differences in the derived Hubble parameter can be large, spanning the range 55 - 80.

The reconstructed value of the Hubble parameter depends on the alignment of the jet, which can be reconstructed from radio images showing a number of lensed features.

The positions of the images of the core are resolved with optical and radio instruments. To identify the source, at least one resolved image is necessary. In the case of gamma-ray observations, the time delay can be measured with a precision of a few percent even when the images are poorly resolved or unresolved. The true source of the variable emissions generally unknown. Figures 7 and 8 demonstrate that changes in the distance between source of variable emission and the core and/or

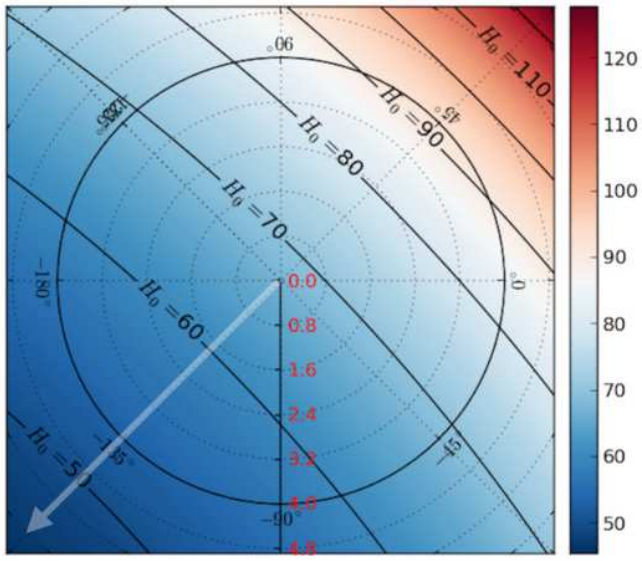

FIG. 7.— A schematic view showing how determination of the Hubble parameter depends on the reconstruction of the location of the variable emitting region. The light arrow indicates the direction towards the center of the lens mass. In this example the source is located at 0.35 Einstein radius from the center of the lens mass. An auxiliary grid is centered at the position of the core. The angular coordinates show the alignment of the jet in the source plane relative to the position of the core. The radial coordinates indicate the distance between the core and the variable emitting region along to the jet, shown as a percentage of the Einstein radius. The contour map shows the value of the Hubble parameter obtained by assuming the position of the core at 0.35 Einstein radius from the mass center of the lens, and time delays corresponding to variable emitting regions at the indicated distances from the core.

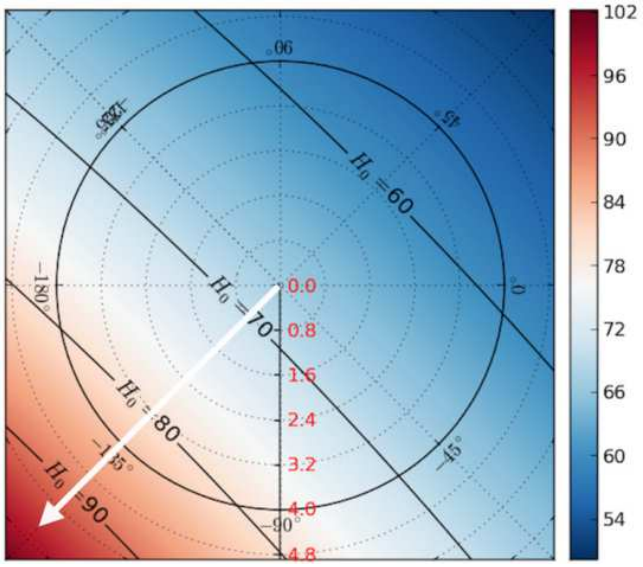

FIG. 8.— The same as Figure 7, but with the core located at 0.7 Einstein radius from the mass center of the lens.

a small error in the positions of a variable core can lead to wide variation in the derived Hubble parameter.

6. DISCUSSION

6.1. *Comparison with Lensing Measurements of H_0*

Time delays between the mirage images of gravitationally lensed variable sources are exploited to estimate the Hubble parameter. The sources which exhibit the most prominent variability over short time periods, and across the entire electromagnetic spectrum, are objects with jets, including, for example, blazars (Ulrich et al. 1997; Ruan et al. 2012).

Figure 5 shows the distribution (gray) of 37 measurements of H_0 using gravitationally lensed systems available in the literature (Table 1). This distribution is characterized by a mean value of 67.95 with an RMS scatter of 12.4 [km s^{-1}Mpc^{-1}].

The red distribution represents the Monte Carlo simulations composed of 4000 trials. For this comparison, we take an offset between the position of the source and the position of the variable emitting region equal to 3% of the Einstein radius. The resulting simulated distribution is characterized by a mean value 67.3 with an RMS scatter of 9.6 [km s^{-1}Mpc^{-1}]. Even for this very simple model, the uncertainty in the reconstruction of the position of the variable emitting region reproduces the scatter and the features in the H_0 measurement distribution obtained from observed gravitationally lensed systems.

An uncertainty in the position of the source in the source plane larger than 1% of the Einstein radius can lead to the same effect as the complex structure of the source, even when the variable emitting region and resolved images spatially coincide (see Figure 6). Note that a typical Einstein radius for these sources is $\sim$ 0.5 arcsecond, and 5% corresponds to 0.025 arcseconds, only twice the HST resolution. Even with HST images, there is a natural limit to reconstruction that can produce a spread in the derived values of H_0.

Table 1 contains a compilation of the H_0 measurements available in the literature. These measurements were obtained using different lens modeling, treatments of the lens environments, and different methods for time delay measurements, with some of the time delays measurement being disputed (Eulaers & Magain 2011). In the future, we expect these effects will be minimized as projects like COSMOGRAIL (Eigenbrod et al. 2005, 2006a,b; Saha et al. 2006; Vuissoz et al. 2007b; Eigenbrod et al. 2007; Vuissoz et al. 2008b; Chantry et al. 2010; Courbin et al. 2011b; Sluse et al. 2012; Tewes et al. 2013a; Eulaers et al. 2013; Tewes et al. 2013b; Rathna Kumar et al. 2013) provide uniform analysis and data for large sample.

All of these differences can contribute significantly to the scatter in H_0 in Table 1. For demonstration purposes of this paper, we take measurements of H_0 at face value. Of course, the other sources of error will change the uncertainty in variability position required to fit the data, but in this work we are concerned with showing what the effect of source variability positional uncertainty is, rather than with quantifying its true contribution to the scatter in H_0 measurements.

The complex structure of the source predicts a very characteristic bimodal distribution, with a dip at the true value. Other systematics may manifest their presence in the distribution of the Hubble constant in different ways. They may shift or broaden the distribution. Thus, in the future, when large samples of H_0 measurements become available, the shape of the observed H_0 distribution will be a useful tool for identifying and quantifying these systematics.

Currently $\sim$ 200 gravitationally lensed systems have been identified. Among them, time delays have been estimated for $\sim$ 20 systems. Future survey instruments like SKA, LSST or Euclid, will increase the number of known gravitationally lensed systems by about two orders of magnitudes. Predictions suggest that LSST alone will provide $\sim$ 4000 time delays (Coe & Moustakas 2009). The distribution of Hubble parameters obtained from these large ensembles of time delays will allow tests of these model of the impact of the complex structure on the derived Hubble parameter. They will also provide a statistical determination of H_0 that can take the complex source structure into account.

6.2. *The Hubble Parameter Tuning Approach*

The measured value of the Hubble parameter is very sensitive to the spatial offset between the position of the core and the position of the variable-emitting region where the time delay originates. Thus, the problem can be inverted. The value of H_0 measured by other techniques can be used to tune the spatial offset between the position of well-resolved images of lensed jets and the position of the variable-emitting region where the time delay originates. We call this approach the Hubble Parameter Tuning (HPT) method for spatially resolving the active region.

The four key components of the HPT method are: the value of the H_0, a model for the lens, the resolved positions of emitting regions, and time delays measured at high energies. We consider each of these issues next.

Currently, various methods of H_0 estimation measure the value of H_0 with an accuracy down to $\sim$2%. However, accounting for the tension between different methods, H_0 is measured with 10% accuracy. In the near future, these methods have the potential for revealing the value of H_0 to 1% accuracy (for a brief review see Suyu et al. 2012).

Modeling of the mass distribution of the lens may be limited by, for example, mass-sheet degeneracy (Schneider & Sluse 2013). Reconstruction of the mass distribution of the lens, in some cases, can be the most constraining element in resolving the spatial origin of variable emission. However, the images of lensed jets are observed with high accuracy from radio, through optical, up to even x-rays with Chandra. The images of emitting regions are resolved at radio with an angular resolution better than 1 milliarcsecond. The morphology of these images is very complex, showing ring structures and multiple images[3]. Thus, lensed jets can help to better constrain the mass distribution of the lens.

Emission from jets can increase by an order of magnitude in a short period of time. The variability time scales (minutes to days) are much shorter than the typical time delays (weeks to years). As a result, time delays can be measured despite poorly resolved, or even unresolved, images.

The HPT approach provides an opportunity, to identify the origin of the variable emission. The answer to this question is crucial at energies where current detectors cannot resolve the sources.

6.3. *Gamma-Ray and X-Ray Observations*

[3] http://www.jb.man.ac.uk/research/gravlens/lensarch/lens.html

Emission from extragalactic variable sources obviously cannot be resolved at gamma-ray energies; the angular resolution of current detectors is limited to $\sim$ 0.1 degree. In this energy range, improvement by a factor of 1000 in angular resolution is required to determine whether the flaring gamma-ray activity originates from a region close to the core or from knots along the jet.

Future gamma-ray detectors will provide an improvement in angular resolution by a factor of a few (Bernard et al. 2014; Wu et al. 2014). Further improvements are physically limited by effects like nuclear recoil. Thus, gamma-ray detectors with a galaxy acting as a lens located along the line of sight to a blazar offer the only way to answer the question of the origin of gamma-ray flares.

In the x-ray, Chandra has an angular resolution of $\sim$ 0.5 arcseconds. The angular resolution in the x-ray allowed the discovery that extragalactic jets have complex x-ray structure, and that the x-ray emission can extend over hundreds of kpcs. The excellent angular resolution of the Chandra instrument enabled the discovery that x-ray flares can originate from distant knots (see example of M87 in Harris et al. 2006).

Even in the x-ray, resolving the sources becomes challenging for more distant sources. Thus, gravitationally lensed x-ray sources offer a way to resolve the emission from jets associated with sources located at high redshift. The study of lensed sources provides a route to investigation of the cosmic evolution of jets.

X-ray detectors like NuSTAR or *Swift*/XRT have an angular resolution of a few arcseconds. Monitoring of x-ray variable gravitationally lensed sources with these instruments can enhance the ability of these instruments to resolve the emission on scales as small as 0.01 arsecend, depending on the properties of the particular lens system.

7. CONCLUSIONS

We use Monte Carlo simulations where we randomly select the position of the core and the jet alignments in the source plane to predict the distribution of values of H_0 obtained from complex lensed variable sources. The only free parameter in our model is the separation between the variable emission region and the core. We investigate the impact of the misinterpreted position of the variable emitting region on the distribution of H_0.

The Monte Carlo simulations successfully reproduce the character of the observed distribution of H_0 derived from individual gravitationally lensed systems. Misalignment by 5% of Einstein radius results in a bimodal distribution of values of H_0 characterized by an RMS of $\sim$ 12 [$\mathrm{km\,s^{-1}Mpc^{-1}}$], similar to the observed RMS of 12.4 [$\mathrm{km\,s^{-1}Mpc^{-1}}$]. Estimation of the Hubble parameter from strongly lensed sources is very sensitive to the position of the region in the lens plane where variability originates. Nonetheless the mean Hubble parameter for a large sample returns the true value.

Other methods determine H_0 to an accuracy of 2%. Thus, we propose taking the value of H_0 from these techniques as given and then using the distribution of H_0 values for gravitationally lensed systems to locate the variable emission regions. In other words, taking H_0 as a known quantity enables the use of gravitational lensing to effectively enhance the resolution of distant variable sources. We call this resolution enhancing approach the

Hubble parameter tuning method for spatially resolving the source of variable emission.

This H_0 tuning approach can be especially useful at energies where the emission from extragalactic sources cannot be spatially resolved due to a poor angular resolution of the detectors. In particular, it can be used at gamma rays where detectors with a galaxy acting as a lens located along the line of sight to a blazar offer the only way to answer the question of the origin of gamma-ray flares. In the x-ray the resolution of current detectors is adequate to resolve nearby extragalactic sources, but application of techniques based on strong lensing enables extension of our knowledge of the structure of these sources to much greater redshift. The method can also be used to enhance the spatial resolution of variable emission even in the optical and NIR, when high resolution images are not available during an outburst, or when the source is located at very high redshift. The extension to large redshift opens the possibility of following the evolution of the source structure with cosmic time, especially when large samples from projects like Euclid and SKA are available.

We thank the referee for valuable comments that prompted improvements in the manuscript. We thank Markus Böttcher, Dominique Sluse, Tommaso Treu, and Jabran Zahid for the valuable comments on the manuscript. A.B. is supported by the Department of Energy Office of Science, NASA & the Smithsonian Astrophysical Observatory with financial support from the NCN grant DEC-2011/01/M/ST9/01891. MJG is supported by the Smithsonian Institution.

REFERENCES

Abramowski, A., Acero, F., Aharonian, F., et al. 2012, ApJ, 746, 151
Aharonian, F., Akhperjanian, A. G., Bazer-Bachi, A. R., et al. 2006, Science, 314, 1424
Auger, M. W., Treu, T., Bolton, A. S., et al. 2010, ApJ, 724, 511
Barnacka, A. 2013, ArXiv e-prints, arXiv:1307.4050
Barnacka, A., Böttcher, M., & Sushch, I. 2014a, ApJ, 790, 147
Barnacka, A., Geller, M. J., Dell'antonio, I. P., & Benbow, W. 2014b, ApJ, 788, 139
Barnacka, A., Glicenstein, J.-F., & Moudden, Y. 2011, A&A, 528, L3
Bernard, D., Bruel, P., Frotin, M., et al. 2014, ArXiv e-prints, arXiv:1406.4830
Bernstein, G., & Fischer, P. 1999, AJ, 118, 14
Biggs, A. D., Browne, I. W. A., Helbig, P., et al. 1999, MNRAS, 304, 349
Biretta, J. A., Sparks, W. B., & Macchetto, F. 1999, ApJ, 520, 621
Biretta, J. A., Stern, C. P., & Harris, D. E. 1991, AJ, 101, 1632
Bolton, A. S., Treu, T., Koopmans, L. V. E., et al. 2008, ApJ, 684, 248
Burud, I., Courbin, F., Magain, P., et al. 2002, A&A, 383, 71
Chantry, V., Sluse, D., & Magain, P. 2010, A&A, 522, A95
Cheung, C. C., Larsson, S., Scargle, J. D., et al. 2014, ApJ, 782, L14
Coe, D., & Moustakas, L. A. 2009, ApJ, 706, 45
Courbin, F. 2003, ArXiv Astrophysics e-prints, astro-ph/0304497
Courbin, F., Chantry, V., Revaz, Y., et al. 2011a, A&A, 536, A53
—. 2011b, A&A, 536, A53
Eigenbrod, A., Courbin, F., Dye, S., et al. 2006a, A&A, 451, 747
Eigenbrod, A., Courbin, F., & Meylan, G. 2007, A&A, 465, 51
Eigenbrod, A., Courbin, F., Meylan, G., Vuissoz, C., & Magain, P. 2006b, A&A, 451, 759
Eigenbrod, A., Courbin, F., Vuissoz, C., et al. 2005, A&A, 436, 25
Eulaers, E., & Magain, P. 2011, A&A, 536, A44
Eulaers, E., Tewes, M., Magain, P., et al. 2013, A&A, 553, A121
Fadely, R., Keeton, C. R., Nakajima, R., & Bernstein, G. M. 2010, ApJ, 711, 246
Fassnacht, C. D., Pearson, T. J., Readhead, A. C. S., et al. 1999, ApJ, 527, 498
Fassnacht, C. D., Xanthopoulos, E., Koopmans, L. V. E., & Rusin, D. 2002, ApJ, 581, 823
Freedman, W. L., & Madore, B. F. 2010, ARA&A, 48, 673
Freedman, W. L., Madore, B. F., Scowcroft, V., et al. 2012, ApJ, 758, 24
Freedman, W. L., Madore, B. F., Gibson, B. K., et al. 2001, ApJ, 553, 47
Gavazzi, R., Treu, T., Rhodes, J. D., et al. 2007, ApJ, 667, 176
Gil-Merino, R., Wisotzki, L., & Wambsganss, J. 2002, A&A, 381, 428
Harris, D. E., Cheung, C. C., Biretta, J. A., et al. 2006, ApJ, 640, 211
Harris, D. E., & Krawczynski, H. 2006, ARA&A, 44, 463
Hjorth, J., Burud, I., Jaunsen, A. O., et al. 2002, ApJ, 572, L11
Jakobsson, P., Hjorth, J., Burud, I., et al. 2005, A&A, 431, 103
Keeton, C. R., Falco, E. E., Impey, C. D., et al. 2000, ApJ, 542, 74
Kelly, B. C., Bechtold, J., & Siemiginowska, A. 2009, ApJ, 698, 895
Kochanek, C. S. 2002, ApJ, 578, 25
Kochanek, C. S., & Schechter, P. L. 2004, Measuring and Modeling the Universe, 117
Koopmans, L. V. E., de Bruyn, A. G., Xanthopoulos, E., & Fassnacht, C. D. 2000, A&A, 356, 391
Koopmans, L. V. E., Treu, T., Fassnacht, C. D., Blandford, R. D., & Surpi, G. 2003, ApJ, 599, 70
Kozłowski, S., Kochanek, C. S., Udalski, A., et al. 2010, ApJ, 708, 927
Lähteenmäki, A., & Valtaoja, E. 1999, ApJ, 521, 493
Lehár, J., Falco, E. E., Kochanek, C. S., et al. 2000, ApJ, 536, 584
Lidman, C., Courbin, F., Meylan, G., et al. 1999, ApJ, 514, L57
Lobanov, A. P. 1998, A&A, 330, 79
MacLeod, C. L., Ivezić, Ž., Kochanek, C. S., et al. 2010, ApJ, 721, 1014
Marscher, A. P. 2008, in Astronomical Society of the Pacific Conference Series, Vol. 386, Extragalactic Jets: Theory and Observation from Radio to Gamma Ray, ed. T. A. Rector & D. S. De Young, 437
Marscher, A. P., Jorstad, S. G., D'Arcangelo, F. D., et al. 2008, Nature, 452, 966
Massaro, F., Harris, D. E., & Cheung, C. C. 2011, ApJS, 197, 24
Matthews, T. A., & Sandage, A. R. 1963, ApJ, 138, 30
Narayan, R., & Bartelmann, M. 1996, ArXiv Astrophysics e-prints, astro-ph/9606001
Oguri, M. 2007, ApJ, 660, 1
Paraficz, D., & Hjorth, J. 2010, ApJ, 712, 1378
Perlman, E. S., Adams, S. C., Cara, M., et al. 2011, ApJ, 743, 119
Planck Collaboration, Ade, P. A. R., Aghanim, N., et al. 2013, ArXiv e-prints, arXiv:1303.5076
Pushkarev, A. B., Kovalev, Y. Y., & Lister, M. L. 2010, ApJ, 722, L7
Rathna Kumar, S., Stalin, C. S., & Prabhu, T. P. 2014, ArXiv e-prints, arXiv:1404.2920
Rathna Kumar, S., Tewes, M., Stalin, C. S., et al. 2013, A&A, 557, A44
Refsdal, S. 1964, MNRAS, 128, 307
Rhee, G. 1991, Nature, 350, 211
Riess, A. G., Macri, L., Casertano, S., et al. 2011a, ApJ, 730, 119
—. 2011b, ApJ, 732, 129
Ruan, J. J., Anderson, S. F., MacLeod, C. L., et al. 2012, ApJ, 760, 51
Saha, P., Courbin, F., Sluse, D., Dye, S., & Meylan, G. 2006, A&A, 450, 461
Savolainen, T., Homan, D. C., Hovatta, T., et al. 2010, A&A, 512, A24
Schechter, P. L. 2005, in IAU Symposium, Vol. 225, Gravitational Lensing Impact on Cosmology, ed. Y. Mellier & G. Meylan, 281–296

Schechter, P. L., Bailyn, C. D., Barr, R., et al. 1997, ApJ, 475, L85
Schneider, P., Ehlers, J., & Falco, E. E. 1992, Gravitational Lenses (Springer-Verlag Berlin Heidelberg New York)
Schneider, P., & Sluse, D. 2013, A&A, 559, A37
—. 2014, A&A, 564, A103
Sereno, M., & Paraficz, D. 2014, MNRAS, 437, 600
Sesar, B., Ivezić, Ž., Lupton, R. H., et al. 2007, AJ, 134, 2236
Siemiginowska, A., Bechtold, J., Aldcroft, T. L., et al. 2002, ApJ, 570, 543
Sluse, D., Chantry, V., Magain, P., Courbin, F., & Meylan, G. 2012, A&A, 538, A99
Suyu, S. H., Marshall, P. J., Auger, M. W., et al. 2010, ApJ, 711, 201
Suyu, S. H., Treu, T., Blandford, R. D., et al. 2012, ArXiv e-prints, arXiv:1202.4459
Suyu, S. H., Treu, T., Hilbert, S., et al. 2013a, ArXiv e-prints, arXiv:1306.4732
Suyu, S. H., Auger, M. W., Hilbert, S., et al. 2013b, ApJ, 766, 70
Tavecchio, F., Maraschi, L., Wolter, A., et al. 2007, ApJ, 662, 900
Tewes, M., Courbin, F., & Meylan, G. 2013a, A&A, 553, A120
Tewes, M., Courbin, F., Meylan, G., et al. 2013b, A&A, 556, A22
Tian, Y., Ko, C.-M., & Chiu, M.-C. 2013, ApJ, 770, 154
Tonry, J. L. 1991, ApJ, 373, L1
Tortora, C., Piedipalumbo, E., & Cardone, V. F. 2004, MNRAS, 354, 343
Treu, T., & Koopmans, L. V. E. 2002, MNRAS, 337, L6
Ulrich, M.-H., Maraschi, L., & Urry, C. M. 1997, ARA&A, 35, 445
Vuissoz, C., Courbin, F., Sluse, D., et al. 2007a, A&A, 464, 845
—. 2007b, A&A, 464, 845
—. 2008a, A&A, 488, 481
—. 2008b, A&A, 488, 481
Walsh, D., Carswell, R. F., & Weymann, R. J. 1979, Nature, 279, 381
Winn, J. N., Kochanek, C. S., McLeod, B. A., et al. 2002, ApJ, 575, 103
Wu, X., Su, M., Bravar, A., et al. 2014, ArXiv e-prints, arXiv:1407.0710
Wucknitz, O., Biggs, A. D., & Browne, I. W. A. 2004, MNRAS, 349, 14
York, T., Jackson, N., Browne, I. W. A., Wucknitz, O., & Skelton, J. E. 2005, MNRAS, 357, 124